Small

NANO · MICRO small
www.small-journal.com

RESEARCH ARTICLE OPEN ACCESS

Cell Culture Substrate Variation Alters Extracellular Vesicle Biogenesis Without Affecting Non-Coding Repeat RNA Profile

Sara I. Veiga[1,2,3,4] | Rebecca L. Porter[1,2] | Berent Aldikacti[1,2,3] | Uma K. Paithankar[1,2] | Kate Calhoun[1,2] | Eric Tai[1,3] | Vishal Thapar[1,3] | Jillian F. Wise[4,5] | David T. Ting[1,2] | Shannon L. Stott[1,2,3,4]

[1]Krantz-Family Center for Cancer Research, Massachusetts General Hospital, Boston, Massachusetts, USA | [2]Department of Medicine, Harvard Medical School, Boston, Massachusetts, USA | [3]Center For Engineering in Medicine and Surgery, Massachusetts General Hospital, Boston, Massachusetts, USA | [4]The Broad Institute of MIT and Harvard, Cambridge, Massachusetts, USA | [5]Department of Biology and Biomedical Science, Salve Regina University, Newport, Rhode Island, USA

Correspondence: David T. Ting (dting1@mgh.harvard.edu) | Shannon L. Stott (sstott@mgh.harvard.edu)

Received: 21 August 2025 | **Revised:** 11 December 2025 | **Accepted:** 19 December 2025

Keywords: extracellular vesicles | mechanosensitive conditions | pancreatic ductal adenocarcinoma | repeat ncRNA | stiffness

ABSTRACT

Tissue stiffening is central to disease progression and aggressiveness in pancreatic adenocarcinoma (PDAC). Here we report how the biomechanical characteristics of the cell culture conditions impact the amount, as well as the cargo, of extracellular vesicles (EVs) produced by pancreatic cancer cells. Cells grown on softer matrices (0.5 kPa) release upwards of 40 times more EVs than those grown on stiffer surfaces (8 kPa) and their cargo is more enriched in protein-coding RNAs related with mitochondrial and cytoskeleton pathways. Moreover, cells grown in a 3D conformation release more EVs than those grown in 2D, with the repeat RNA content being maintained across all different cell culture conditions. Our study provides evidence to support that the mechanical microenvironment of cells influences EV generation, with distinct consequences for coding and non-coding RNA packaged within the EVs.

1 | Introduction

Cancers develop in highly complex environments with diverse characteristics that contribute to tumor progression. The extracellular matrix (ECM) that surrounds the tumors provides structural support and mechanical cues for cell growth, and in most solid tumors, increased ECM stiffness contributes to metastasis, cell invasion, angiogenesis, and immune escape [1]. Pancreatic ductal adenocarcinoma (PDAC) is characterized by high stiffness, ranging from 4 to 6kPa [2–4], due to the extensive stromal desmoplastic response and matrix stiffness, which is a defining feature of PDAC tumors that is associated with metastatic propensity, resistance to therapy, and poor prognosis [2].

Much of our early understanding of cancer pathophysiology has come from the study of cancer cells growing adherently as monolayers (2D) in culture dishes, but there has been a greater appreciation of the importance of 3D culture systems that more closely recapitulate tumors in vivo including cell morphology and behavior, responses to therapy, and adaptive growth mechanisms [5–8]. At the transcriptome level, cancer cells growing in 3D, when compared with 2D culture, show significant differences in gene expression [9, 10]. In addition to 2D versus 3D culturing,

Sara I. Veiga, Rebecca L. Porter, Berent Aldikacti and Uma K. Paithankar contributed equally to this work

alterations in the mechanical properties, including the elasticity of the substrate cells are grown on, can alter expression profiles, cell differentiation and functional phenotypes [11–15]. Despite this knowledge, we consistently use static models in our labs that do not reflect the characteristics of tissues in our body or in tumors.

In the field of extracellular vesicles (EVs), the effects that different variables in culture conditions may have on in vitro generated EVs has not been extensively studied [16–18]. EVs consist of a diverse group of particles that incorporate many characteristics of the origin cells from which they are released. These cargo can include proteins, lipids, DNA and RNA molecules [19], and EVs serve as an important means of local and distal intercellular communication through the transfer of their cargo to recipient cells [20, 21]. EVs are abundantly produced by tumor cells and contribute to tumorigenesis, angiogenesis, invasiveness, and metastasis by altering the cellular microenvironment in the tumor and at metastatic sites [22–27]. In particular, tumor-derived EVs have been found to carry a variety of non-coding RNAs (ncRNA), some of which mediate their influence on tumor cells and the tumor microenvironment, and have potential as specific biomarkers for liquid biopsies [28–33]. While these ncRNAs have not been extensively studied in the EV field, it has been suggested that their enrichment in EVs can be a regulated mechanism [34]. We have previously reported the aberrant expression of typically silenced repeat ncRNAs in epithelial cancer cells, comprising up to 50% of all cellular transcripts in murine and human PDAC [35]. Repeat ncRNAs encompass retrotransposons (i.e., LINEs, SINEs), human endogenous retroviruses (ERVs), and satellite repeats; the expression of some satellite repeat RNAs is exquisitely specific for cancer cells. Subsequent work from our group and others has clearly demonstrated an immunomodulatory role of repeat RNAs expressed in cancer cells through their ability to stimulate innate immune responses and activate interferon signaling [36–40]. Given their predominance in cancer cells and the important implications of their expression, understanding how loading of repeat ncRNAs into EVs is affected by their environment could clarify how the mechanical properties contribute to disease progression.

While EVs have a recognized role in cancer, up to now, most studies looking into EV cargo and roles in physiological processes are based on vesicles derived from cells cultured in 2D plasticware. In the recent years, several studies have worked to address this issue, with one group showing that 3D cell culture stimulates EV biogenesis and the secretion of EVs with characteristics more similar to in vivo, thus strengthening the idea that biomimetic culture conditions are crucial to reflect the in vivo EVs [16]. Additionally, studies focused on substrate stiffness have shown that EV biogenesis and cargo are affected by the mechanical stiffness of the culture conditions [17, 18, 41, 42]. However, when looking into the cell culture effects on cargo, these studies usually focus on proteomic analysis and evaluation of protein content, but do not address gene expression alterations.

In the present study, we aim to define the RNA content of PDAC-derived EVs and determine the effect of different cell culture methods on their biogenesis and composition. We took advantage of the unique characteristics of these PDAC cells, that were previously established in our laboratory, from ascites of pancreatic adenocarcinoma patients [43]. Depending on the substrate provided, these cell lines have the ability to grow both as 2D monolayers (adherent plates) and 3D spheroids (non-adherent plates), using suitable media formulations. Accordingly, they are a robust model to study the same cells under varying culture conditions, instead of introducing additional variables such as mechanical confinement, gene editing or major changes in culture medium. Analysis of overall RNA content of EVs released by PDAC cell lines using total RNA-Seq revealed an enrichment of non-coding repeat RNAs compared with the transcriptome of parental cells in both 2D and 3D cultures. Notably, we identify a significant increase in EV generation in 3D compared to 2D cultures. This is associated with the relative stiffness of the substrate that PDAC cancer cells grow on which has implications on the contribution of biophysical properties of the tumor microenvironment on EV pathogenesis.

2 | Results

2.1 | EV Characterization and RNA Content Assessment Between EVs and Parental Cells

To fully define the RNA content of PDAC EVs, we utilized patient-derived cell lines generated from the ascites fluid of patients with metastatic PDAC [43]. For these studies, we chose two cell lines, one more mesenchymal (PDAC3) and another more epithelial (PDAC8) [44]. Each PDAC cell line was grown in standard adherent 2D culture conditions and supernatant was collected at 50–70% confluency. EVs were then isolated following ultracentrifugation in which supernatant was centrifuged for 2 h at 100,000 x *g*. (Figure 1A). Following the MISEV23 guidelines [45], a series of quality checks was done to ensure that a purified population of EVs were collected for further use in our studies. Isolated EVs were characterized by Western blot and showed enrichment in classic EV markers (ALIX and CD9) and absence of cell contaminants such as endoplasmic reticulum protein Calnexin (Figure 1B; FigureS1), satisfying MISEV recommendations for evidence of detectable presence of EVs in our samples. The tetraspanin protein content of these EVs was further characterized by using dSTORM imaging (Figure 1C), with CD9, CD63, and CD81 detectable at the EV surface. Together, these experiments confirmed the presence of EVs in our isolated samples. Moreover, further characterization of the EVs by transmission electron microscopy (TEM) showed classic EV-shaped structures of around 100 nm (Figure 1D).

EVs were then lysed and homogenized in Qiazol buffer, and RNA was extracted and subjected to total RNA-sequencing (RNASeq) (Figure 2A). The transcriptomes of the PDAC cell lines were compared with the transcriptome of their corresponding isolated EVs. Compared with their parental cell transcriptome, our isolated EVs possess detectable differences in RNA content with respect to specific transcripts (Figure 2B; Figure S1A) and enrichment of cancer-associated pathways (Figure 2C; Figure S1B). These data suggest that RNAs are selectively loaded into EVs rather than simply reflecting the same composition of RNAs in the cytosol of the cells. Given previous findings on non-coding RNAs (ncRNAs) [32, 33], we next determined the ncRNA profile of tumor cells and EVs by mapping RNASeq reads to the human genome (hg38) and Repbase using the STAR aligner [43], followed

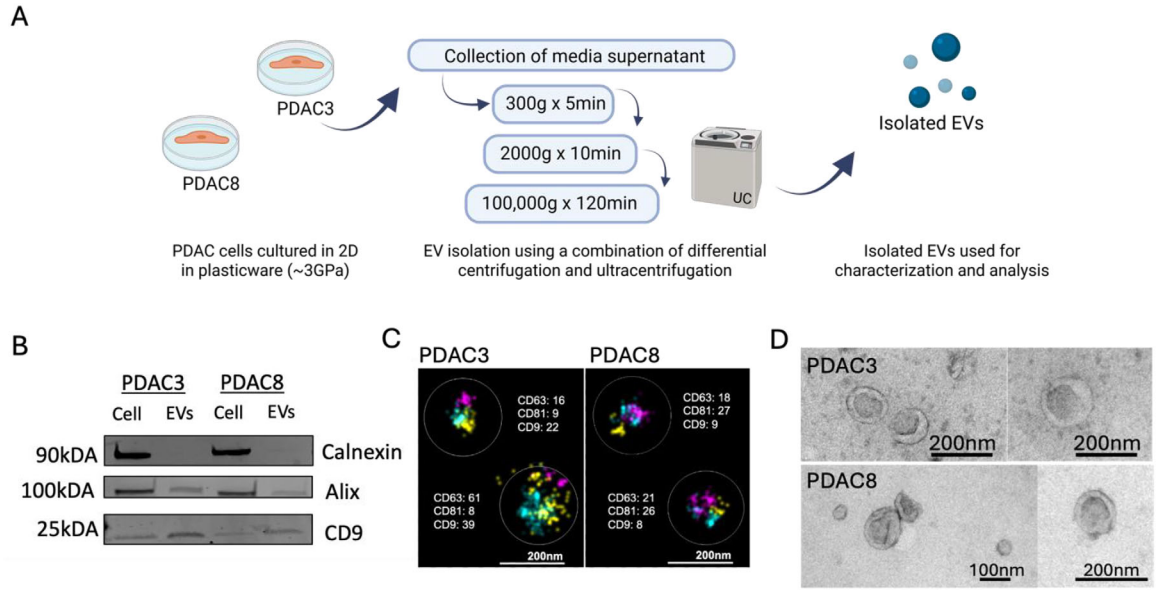

FIGURE 1 | Characterization of EVs isolated from patient-derived cell lines (A) Graphical abstract shows the process, from PDAC cell culture in 2D plasticware surfaces (~3 GPa), to cell supernatant collection and EV isolation using ultracentrifugation. (B) Western blot shows the presence of ALIX and CD9, common EV markers, and absence of Calnexin, an endoplasmic reticulum protein. (C) Using dSTORM for single molecule imaging, the presence of traditional EV proteins was assessed to affirm EV status: CD9-AF488 (yellow), CD63-AF555 (blue) and CD81-AF594 (pink). In the micrograph, two vesicles are shown, and numbers represent the number of dots detected in each vesicle and are proportional to the protein expression at the EV surface (scale bars are 100 and 200 nm). (D) TEM image shows distinct vesicles present in our PDAC3 and PDAC8 preparations, further confirming efficient purification of EVs (scale bars are 100 and 200 nm).

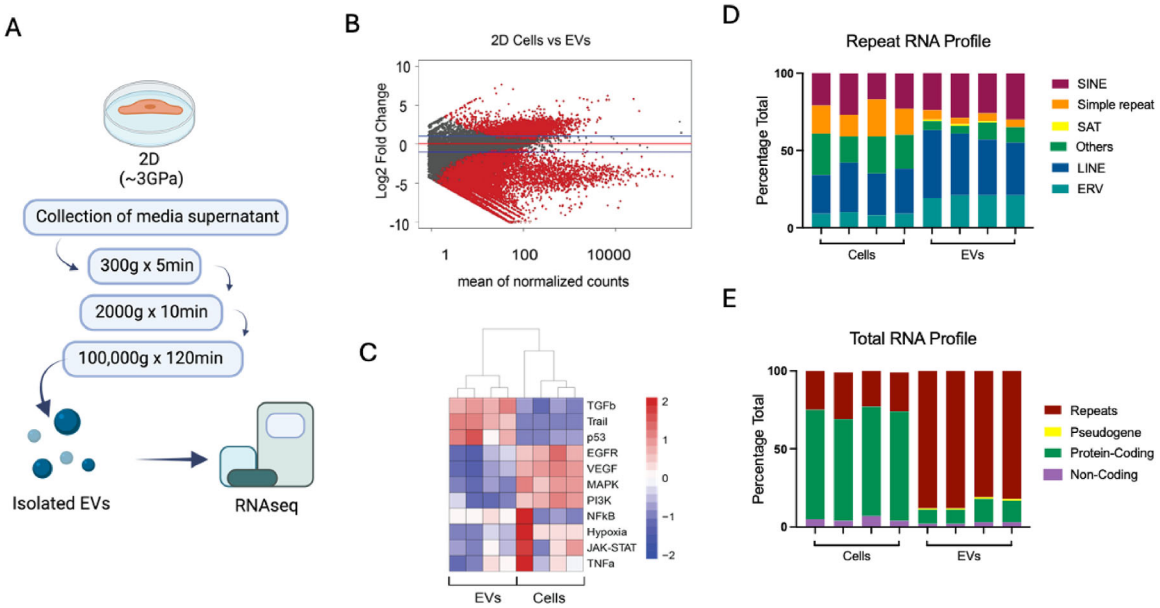

FIGURE 2 | Total RNA-seq analysis shows differential packaging of RNA subtypes into EVs compared to their cell of origin. (A) Graphical abstract shows the process, from PDAC cell culture in 2D plasticware surfaces (~3 GPa), to cell supernatant collection and EV isolation using ultracentrifugation, followed by RNA-seq. (B) Differential expression analysis was done, and the MA plot plotted in the direction of Cell vs. EVs using DESeq2 package in R. Cell and EV sequencing results from two cell lines were pooled individually and treated as replicates for this analysis. Each dot represents a single gene of input, and the differentially expressed genes are shown in red (FDR <0.05). (C) Heatmap of pathway analysis of 11 cancer-associated pathways by Progeny in R. Analysis shows differential packaging of RNA into EVs compared to their cell of origin. (D) RNA subtypes pooled into four groups. Repeats, Pseudogene, Protein-Coding, and Non-Coding) (Color legend is shown on the right). Relative expression of four subtypes of EV and cellular RNA is shown as a percentage of raw counts. The RNA content of cells and EVs shows that non-coding RNA is differentially packaged into EVs, and it is dominated by Repeat RNA. (E) Repeat RNA was further divided into six groups. (SINE, Simple repeat, SAT, Others, LINE, ERV) (color legend is shown on the right). Total RNA sequencing was performed with a minimum of two biological replicates.

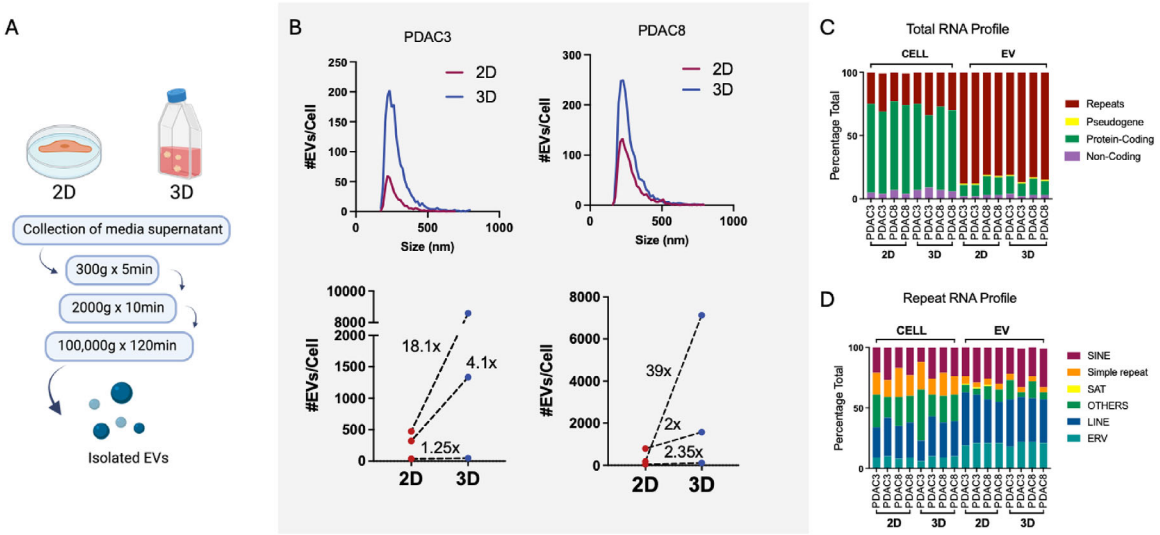

FIGURE 3 | Size, concentration, and transcriptome characterization of EVs and parental cells cultured in 2D monolayer and 3D spheroid models. (A) Graphical abstract shows the process, from PDAC cell culture in 2D plasticware surfaces (~3 GPa) and a 3D spheroid-like conformation, to cell supernatant collection and EV isolation using ultracentrifugation. (B) Graphs shows EV size (top) and numbers (bottom) for PDAC3 and PDAC8-derived EVs. Data was obtained by tunable resistive pulse sensing (TRPS). EV size distribution is shown by a representative TRPS line graph at the top (n = 3 independent captures, mean ± S.D). The normalized concentration of paired experiments is shown with dashed line at the bottom (n = 3 independent experiments, mean ± S.E.M). (C) Total and (D) repeat RNA profiles are shown as percentages of total raw counts from EVs isolated from 2D and 3D conditions. Total RNA sequencing was performed with a minimum of two biological replicates.

by annotation with Gencode and repeatmasker. This method allows for detection of repetitive elements often omitted from standard RNASeq alignment protocols [46]. We had previously shown that PDAC cell lines produce EVs enriched in repeat ncRNAs as compared to their parental cells [32]. These results were recapitulated in this study, where we see an enrichment of repeat ncRNAs in EVs compared with parental cells, with more than 70% of the total reads derived from repetitive sequences in EVs (Figure 2D). Further characterization of repeat RNA subclasses revealed that within the repeat ncRNA family there is specific enrichment for Long Interspersed Nuclear Element (LINE), Short Interspersed Nuclear Element (SINE), satellites (SAT), and Endogenous Retroviruses (ERVs) in EVs compared with parental cells, which contain proportionally more simple repeats and other/unannotated repeats (Figure 2E). This abundance of repeat ncRNAs, particularly LINE, SINE, and ERV elements, and relative lack of mRNAs in EVs was observed in each of the cell lines tested, suggesting this is a common feature of PDAC derived-EVs.

2.2 | Cell Culture Substrate Variation Alters EV Production and Repeat RNA Content Enrichment

Due to the growing interest in cancer derived-EVs as blood-based biomarkers and as a mechanism to transfer information within the tumor microenvironment, it is critical to understand the effects of different growth conditions on EV generation and content to guide future investigations. Therefore, we next asked whether culturing these tumor cells under adherent (2D) or non-adherent (3D) conditions alters the number and size of released EVs, as well as the EV-RNA content (Figure 3A). For each cell line, an equal number of cells were used to initiate cultures, and the entire volume of supernatant was collected for EV isolation by differential ultracentrifugation. Supernatant was collected from 50–70% confluent 2D cultures and at day 5 for 3D cultures. EV size and number were quantified using a tunable resistive pulse sensing (TRPS) qNano instrument as previously described [47]. Cells in culture were counted at the time of EV collection, and the number was used to normalize EVs. An increased number of EVs per cell were generated from 3D conditions compared with 2D across both PDAC cell lines tested (Figure 3B). While the average EV size varied slightly between cell lines, the cell line-specific EV size was maintained between 2D and 3D culture, indicating that 3D culture conditions promote the release of more EVs that are similar in size to those released from 2D culture. Total RNA profile revealed again an enrichment of repeat RNAs for both 2D and 3D conditions, while the loading of protein-coding RNA into the EV cargo was notably depleted (Figure 3C,D). In addition, there were detectable differences in overall RNA content between cells grown in 2D vs. 3D cultures and the EVs isolated from each condition (Figures S1A and S2A). These data suggest that the PDAC cancer cell lines grown under 3D conditions produce a higher number of EVs per cell, without majorly affecting the ncRNA cargo profiles.

Cancer tumors possess inherent differences in stiffness within and across cancer types, depending on the composition and abundance of stroma [48]. Therefore, we were interested in exploring the effect of culture substrate stiffness on generation and content of tumor derived-EVs using our in vitro PDAC cell line culture system. To accomplish this, cells were cultured on hydrogels that can be tuned to present cells with a range of substrate stiffnesses as previously described [49]. Pancreatic cancer tissue stiffness usually ranges from 4 kPa to 8kPa [2–4], and therefore, we decided to choose stiffness values that were lower, and representative of an in-between range (0.5 kPa, 2 kPa and 8 kPa), with attention to what was commercially available and thus, fully characterized.

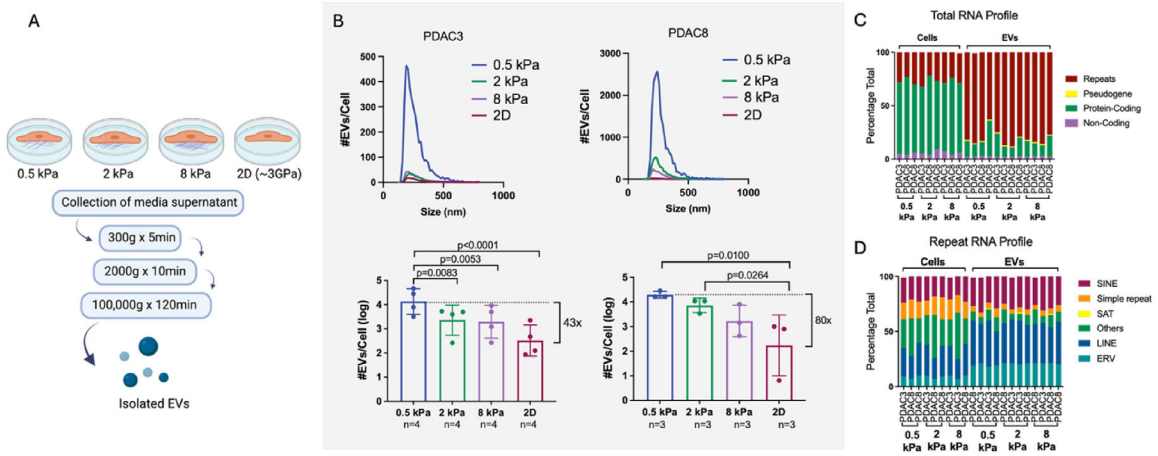

FIGURE 4 | Size, concentration, and transcriptome characterization of EVs and parental cells cultured in hydrogels of different stiffness. (A) Graphical abstract shows the process, from PDAC cell culture in hydrogels of different stiffness (0.5, 2, and 8 kPa), to cell supernatant collection and EV isolation using ultracentrifugation. (B) Graphs shows EV size (top) and numbers (bottom) for PDAC3 and PDAC8-derived EVs. Data was obtained by tunable resistive pulse sensing (TRPS). EV size distribution is shown by a representative TRPS line graph at the top (n = 3 independent captures, mean ± S.D). The normalized concentration is shown by dot plots with an overlayed box plot to show the mean at the bottom (n = 3 independent experiments, mean ± S.E.M). (C) Total and (D) repeat RNA profiles are shown as percentages of total raw counts from EVs isolated from 0.5, 2, and 8 kPa conditions. Total RNA sequencing was performed with a minimum of two biological replicates.

Our adherent 2D culture system used up to this point comprises regular laboratory plasticware, which has a stiffness on the order of 1 GPa to 10GPa [50, 51]. Supernatant was collected from cells grown on hydrogels with defined stiffness levels, and EVs were isolated through ultracentrifugation (Figure 4A). EV number and size were determined on the qNano instrument and normalized to cell number at the time of collection (see Methods). As demonstrated in Figure 4B, cells grown on the softest substrates (0.5 kPa) produced 40 times more EVs when compared with stiffer (8 kPa) surfaces. Similar to the findings between 2D and 3D culture, changing the stiffness of the substrate altered EV number without significant differences in EV size, in both PDAC cell lines. EVs isolated from these cells were also measured using Nanoparticle Tracking Analysis (NTA), which confirmed higher EV generation from softer hydrogels and conservation of EV size distribution (Figure S3A,B). Total RNASeq from cells and EVs revealed several differences in overall RNA content between soft and stiff substrate conditions (Figures S1A and S2B). With respect to the total RNA profile, there was a consistent enrichment of repeat ncRNAs in EVs compared with cells which was comparable in magnitude across all substrate stiffnesses (Figure 4C). Once again, this enrichment was specifically observed in the LINE, SINE, SAT, and ERV subclasses (Figure 4D). Taken together, these data indicate that growing PDAC tumor cells under non-adherent conditions and under adherent but less stiff substrate conditions leads to increased EV production but preserves EV size and EV non-coding RNA content as well as the enrichment of certain subclasses of repeat ncRNAs within the vesicles.

2.3 | Culture Stiffness Impacts Protein-Coding Cargo in EVs

Considering the enrichment in repeat ncRNA content within EVs was not significantly affected by the different cell culture conditions, we set out to investigate how the protein-coding cargo changes across EVs derived from cells grown in different culture substrate/stiffness conditions. Data analyses show that several genes were differentially expressed across all the stiffness conditions in EVs isolated from PDAC3 and PDAC8 cells when compared with 2D; however, only EVs from cells grown on the softest hydrogels, i.e., 0.5 kPa, had statistically significant (adjusted p-value < 0.05) differentially expressed genes (DEGs) (Figure 5A; Figure S4). We identified 989 genes that were enriched in softer (0.5 kPa) hydrogels compared to plastic (2D). Gene-Set Enrichment Analysis (GSEA) comparisons of 0.5 kPa to 2D revealed an upregulation of various mitochondrial processes related to gene expression, respiration and ATP synthesis (Figure 5B). Despite not reaching significant levels, cytoplasmatic translation, as well as ribosome biogenesis and assembly, were identified as potential biological processes in 2 and 8 kPa stiffness (Figure S5A). Downregulated processes were biologically discrete and include cell adhesion, homeostasis, and signaling pathways (Figure 5B). A curated list of genes with biological relevance, identified from Differential Gene Expression (DGE) and GSEA results, was selected for further analysis and a heat-map was created across all conditions (Figure 5C). EVs obtained from PDAC3 cells revealed several variations in content between the conditions, with mitochondrial, cytoskeletal, and transcriptional regulation-associated genes more enriched in the softer hydrogels while the chemotaxis-related genes were more enriched in the stiffer conditions (Figure 5C). Interestingly, the 3D cell culture conditions were comparable with 2D culture conditions for this selected set of genes. However, for the PDAC8 cell line, when taking a similar analytical approach for these particular categories of biological relevance processes, we found the data to have more variability across replicates (Figure S5B). In the interest of evaluating if the cell culture mechanical differences would translate into mechano-transduction signaling changes in the EV cargo, we further analyzed a curated list of genes from GSEA mechano-associated biological processes (Figure S5C). This showed that cell culture changes do not seem to

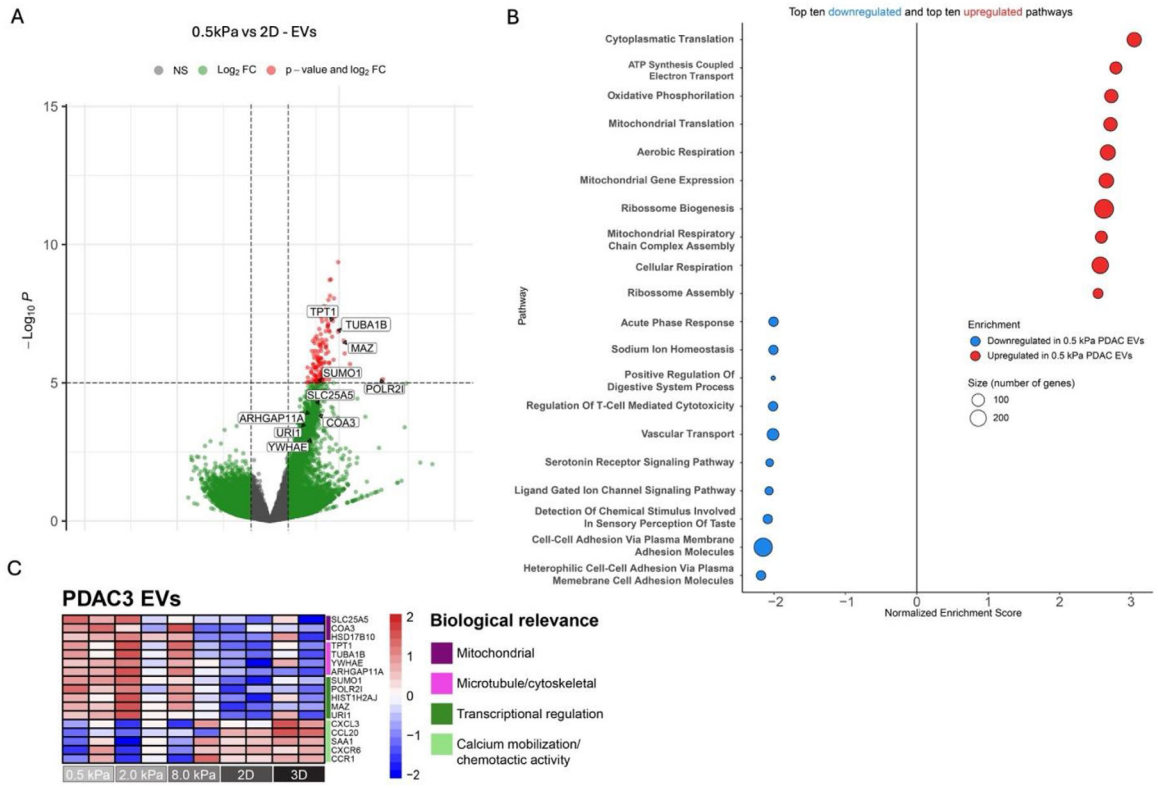

FIGURE 5 | Biological relevance and pathway enrichment for PDAC EVs. (A) Volcano plots show the transcriptomic analysis of EVs isolated from 0.5 kPa compared with 2D culture conditions. Genes of interest are highlighted in the plot. (B) Bubble plot of Gene-Set Enrichment Analysis (GSEA) for the Gene Ontology Biological Processes gene set of PDAC3 and PDAC8 EVs isolated from 0.5 kPa v 2D conditions. In total, this GSEA yields 94 biological processes significantly downregulated and 165 biological processes significantly upregulated in 0.5 kPa PDAC EVs; here, the top ten downregulated and top ten upregulated biological processes are depicted. The size of the bubble is proportional to the size of the gene set. The color of the bubble indicates the pathway upregulation (red) or downregulation (blue) in PDAC EVs isolated from 0.5 kPa compared to 2D culture conditions. (C) Heatmap with curated gene set for PDAC3 EVs across all cell-culture substrate stiffness conditions. For the gene set curation, genes were extracted from DGE and GSEA results. Log-2 normalization was applied prior to heatmap generation.

significantly impact biomechanical associated pathways, suggesting that the mitochondrial, cytoskeletal and transcriptional associated changes observed are genuinely associated with cell culture stiffnesses changes.

Overall, the vesicle protein-coding RNA content seems to be dependent on the matrix that the cells are cultured in.

3 | Discussion

It is now well established that EVs carry bioactive molecules including proteins, lipids and a variety of RNA species which can be transferred to recipient cells as a means of intercellular communication [52]. Whether the content of EVs is a stochastic representation of the RNA content of their parental cells versus a consequence of specific loading into the vesicle remains an area of interest in the field. Recent evidence has suggested that mRNA and miRNA transcripts and proteins are differentially represented between EVs and their parental cells [53–55]. Furthermore, molecules related to protein [56] and miRNA [54] loading identified within EVs, suggesting that cargo is selectively loaded into EVs. Our results are in concordance with this, as we observed differences in the relative abundance of the different subclasses of RNA molecules between EVs and their parental cells. Notably, by performing total RNASeq with computational platforms that allow detection of repetitive elements, we show that most of the RNA contained within EVs is repeat RNAs, whereas the parental cells are carrying primarily protein-coding mRNA molecules. Further, this enrichment of repeats was preserved across all culture conditions studied, suggesting this is likely a conserved phenomenon. These findings extend the current knowledge in the field, which has been largely focused on mRNA, miRNA and short non-coding RNAs to date. More recently, there has been increased interest in vesicular long non-coding RNAs (lncRNAs) as well, which are enriched in certain EV types [57, 58]. The cancer-specific human satellite II (*HSATII*) RNA has been detected in PDAC patient plasma and found to exist predominantly within the EV fraction [59], indicating that repeat RNAs may be a generalizable finding in many tumor-derived EVs [32, 33]. However, a comprehensive analysis of repeat RNAs in EVs has remained elusive, largely because of the limited coverage of repeat sequences in microarray technology and the failure to capture most subsets of repeats using standard poly(A)-based RNA-Seq protocols [46]. Here, we show the value of combining Total RNASeq and mapping of reads to both RepeatMasker and Repbase to comprehensively define the repeat transcriptome of PDAC cells and the EVs they generate. The high abundance of

repeat RNAs in PDAC-derived EVs is not entirely unexpected as it is known that epithelial cancers, including PDAC, massively overexpress many classes of repeat RNAs [35, 60, 61]. In cells, it is known that repeat RNAs, especially satellites [40], LINE-1 [62] and HERVs [36, 38], activate viral recognition pathways and induce an interferon response. Therefore, it is likely that tumor cells acquire adaptive mechanisms to tolerate repeat RNA expression and avoid triggering a suicidal immune response.

Based on our findings, it is intriguing to consider export of repeat RNAs packaged in EVs as an additional strategy for cells to survive under high repeat RNA stress. Further studies into the regulation of repeat RNA expression in tumor cells and their EVs, as well as the consequences of inhibiting their packaging into EVs, are necessary to confirm this hypothesis.

In addition to the potential biological relevance of vesicular non-coding RNA, we also investigated how cell culture conditions can influence the protein-coding cargo in PDAC tumor-derived EVs despite decreased enrichment in these vesicles. We observed that cell culture conditions seem to influence protein cargo loading, with varying biological pathways being enriched in different conditions. Softer conditions seemed to favor cellular pathways such as cytoskeletal and transcriptional, while stiffer pathways were enriched for tumor environment modifying pathways such as chemotaxis. Similar results have been observed by another group [18] that proposed that EVs from stiffer matrix would have a microenvironment remodeling role while EVs from softer subtracts would focus on primary tumor growth.

Furthermore, this study, as well as others [16–18, 63, 64], shows that the biomechanical conditions in which different cells are cultured affects not only their EV cargo, but the quantity of EVs generated per cell. Cells cultured in 3D release more EVs than those derived from 2D culture, across multiple cancer types, and it has been shown that 3D-culture-derived EVs are more similar to patient plasma samples than those derived from cells cultured in 2D [16, 63, 64]. While the effects of 3D conformation on EV biogenesis and cargo are in accordance with ours, our study shows that cells cultured on softer substrates (0.5 kPa) release more EVs per cell than the stiffer substrates. We note that our results differ from what others have published in prior work [17, 18]. Specifically, for other cell lines, they reported an increase in EV production when cells were cultured on stiffer substrates ($\geq$ 10 kPa) [17, 18]. One group hypothesized that this may be due to the increase in cell density between the different conditions, resulting in more EVs [18]. For our work, our data is normalized to the number of cells present for each condition. Specifically, for each data point, we enumerated the number of cells in culture at the time of media collection and normalized our EV data accordingly (see Methods). Without normalization (looking at averages across conditions without consideration of cell number), we observed similar trends to the work previously described.

Nonetheless, our study shows that manipulating cell culture conditions can have an important and significant impact on EV generation and cargo. This can directly affect the ability to use EVs in clinical therapeutical applications, where EV slow release is a critical limitation and scalability and efficiency are crucial for success. The knowledge about the effects of culture mechanical properties can help to better design systems for high yield EV production within bioreactors, which has started to be explored by others [65–67].

In light of these in vitro findings, the relative efficiency of EV generation by cancers with different stiffness and by tumors with varying degrees of stroma within a cancer type may be assumed to be different. This is an important consideration if EVs are to be developed as biomarkers, given that chemotherapeutic agents [68] and radiation [69] target both the tumor cells and the tumor microenvironment and result in alterations of the physical properties of the tumor.

4 | Conclusion

Our findings demonstrate that for our patient-derived cell lines, the RNA proportions within EV cargo is relatively fixed with a predominance of repeat RNAs, irrespective of whether they are released from cells in adherent versus non-adherent culture or from cells grown on adherent substrates of varying stiffness. Interestingly, PDAC cells grown in 3D and in 2D on hydrogels with lower elasticity generated a higher number of EVs compared with cells grown in 2D on classic culture plastic. However, the predominance of repeat RNAs in EVs was maintained across all conditions, suggesting that culture and growth conditions do not affect the genomic information carried by EVs, and this may be a conserved process. The finding that EV production can be increased through manipulation of culture matrices, might be of value for applications related to EV bioreactor design. Nonetheless, we observed that EVs from the different substrate culture conditions have different coding cargo than those derived from cells cultured in plasticware. Softer substrates (0.5kPA) are more enriched in protein-coding RNA related with mitochondrial and cytoskeletal pathways as well as transcriptional regulation and chemotactic activity. This suggests that biological information may be differentially packaged on the EVs as disease progresses. Further studies are required to elucidate the molecular mechanisms linking these biomechanical variables to the effects on EV generation. Our observations support the hypothesis that EVs are differently generated by tumors in different stages, and the understanding of their cargo variations according to disease progression can help us to better understand and guide biomarker discovery for disease monitoring.

5 | Materials and Methods

5.1 | Cell Culture

PDAC 3 and PDAC8 cell lines were generated and provided by the Ting laboratory at Massachusetts General Hospital [43]. The 2D cell line models for PDAC3 and PDAC8 were cultured in DMEM (Gibco, Thermo Fisher Scientific, Waltham, MA) with 10% Exosome-depleted fetal bovine serum (System BioSciences, Palo Alto, CA) and 1% penicillin/streptomycin (Gibco, Thermo Fisher Scientific). Tissue-treated plastic flasks (Corning, Corning, NY) and 0.5 kPa, 2 kPa, and 8 kPa hydrogel plated and collagen-coated plates (Matrigen, Irvine, CA) were used for the 2D culture experiments. The 3D cell line models for PDAC3 and PDAC8 were cultured in RPMI 1640 (Gibco, Thermo Fisher Scientific), 2% B27 (50x, Gibco, Thermo Fisher Scientific), 0, 025% EGF/FGF

(100 ng/μL), and 1% penicillin/streptomycin (Gibco, Thermo Fisher Scientific). Ultra-low attachment surface 6-well plates (Corning) were used for culture. All cells were grown at 37°C with 5% CO^2. 2D cultures were established by seeding 60K cells/well in 6-well plates and 3D cultures were started with 100K cell/ 6-well plates. Cells were counted using the Cellometer Auto T4 (Revvity, Waltham, MA) TrypLE Express (Gibco, Thermo Fisher Scientific) was used to detach cells for subculture in the 2D model, as well as to dissociate the spheroids in the 3D models, every 2 weeks, to prevent increased apoptosis in the nutrition starved core of the spheroid. After collection of cell conditioned media for EV isolation, cells were dissociated and counted using a brightfield microscope.

5.2 | EV Isolation and Measurement

EVs were isolated from the conditioned medium of PDAC3 and PDAC8 cells cultured under 2D and 3D conditions. The conditioned media collected from each model was centrifuged at 300 x *g* for 5 min to eliminate dead cells, supernatant was collected and followed by a 2000 g spin for 10 min to eliminate cell debris. Collected supernatant was filtered through a 0.8 μm filter and ultracentrifuged at 100 000 x *g* for 90 min (Optima L-90K Ultracentrifuge, Beckman-Coulter, Brea, CA). The EV-pellet was resuspended with 0.22 μm double-filtered PBS and split for EV characterization, quantification, and RNA isolation.

5.3 | Western Blot

Cell lysates were prepared using 1x RIPA buffer with protease inhibitor (Halt Protease and Phosphatase Inhibitor Cocktails, Thermo Fisher Scientific), on ice for 15 min. Sample was clarified by centrifugation at 12 000 x *g* for 10 min at 4°C, and supernatant harvested for protein collection. Cell lysates and EVs were normalized based on protein loading. Protein quantification was performed using MicroBCA Protein Assay kit (Thermo Fisher Scientific). 5 μg of cell lysates or EVs were boiled with 4X Laemmli sample buffer (Bio-Rad), with β-mercaptoethanol (Sigma Aldrich) added as reducing reagent, for 5 min at 95°C. Samples and molecular weight markers were subjected to SDS-PAGE and then transferred to a PVDF membrane using the Trans-Blot Turbo Transfer System (Bio-Rad, Hercules, CA). Membranes were blocked with Intercept (TBS) Blocking Buffer (LI-COR Biosciences, Lincoln, NE) for 1 h at RT, and primary antibodies incubated in Intercept T20 (TBS) Antibody Diluent (LI-COR Biosciences) overnight at 4°C. Membranes were washed with TBST (1x Tris containing 0.1% tween-20) for 5 min 3 times and incubated with IRDye Secondary Antibodies (LI-COR Biosciences) for 1 h at RT. Images were developed using Odyssey CLx (LI-COR Biosciences).

5.4 | Antibodies and Concentrations for Western Blot Analysis

The following antibodies were used: CD9 (Biolegend, cat# 312102) 1:500; Alix (E6P9B) (Cell Signaling Technology, Danvers, MA, cat#92880S)1:500 and Calnexin (C5C9) (Cell Signaling, cat# 2679P) 1:500. Goat Anti-Mouse IgG Polyclonal Antibody (IRDye 800CW) (LI-COR Biosciences, cat# 926–32210) 1:5000, Goat Anti-Rabbit IgG Polyclonal Antibody (IRDye 680RD) (Li-COR Biosciences, cat# 926–68071) 1:5000.

5.5 | Direct Stochastic Optical Reconstruction Microscopy (dSTORM) of EVs

The tetraspanin (CD9, CD63, CD81) content of EVs was investigated using super resolution microscopy (dSTORM) through the Nanoimager system (Oxford Nanoimager, Oxford, England). For this, we employed the EV Protein Profiler kit (cat. # EV-MAN-1.0, ONI). The ONI microfluidic chip provide in the kit was functionalized for EV immobilization, according to the protocol recommended by the manufacture, using CD9, CD63 and CD81 capture antibodies provided in the kit. After blocking, the EV sample was run through the device channels for EV capture. Channel was washed and captured EVs were fixed. The tetraspanins at the surface of the captured EVs were tagged using a combination of CD9-AlexaFluor488 (CD9-AF488), CD63-AlexaFluor555 (CD63-AF555) and CD81-AlexaFluor630 (CD81-AF630) fluorescent antibodies. The microfluidics chip with the stained EVs was imaged under the ONI microscope using an imaging buffer provided in the kit and adequate for dSTORM imaging. The tetraspanin composition of EVs was analyzed using the CODI software, following analysis guidelines recommended by the manufacturer.

5.6 | TEM Imaging

PDAC3 EV samples were fixed with 4% glutaraldehyde and diluted 1:10 with 1× PBS. Each sample (10 μl) was transferred onto a 200-mesh Formvar/carbon-coated nickel grid and allowed to adsorb for 15 min. Grids were blotted (to remove excess suspension solution) and contrast stained for 30 to 60 s using tylose+uranyl acetate solution. Grids were blotted again, rinsed once with filtered distilled deionized water, and, allowed to dry after blotting residual liquid. Analysis of the preparations was done using a JEOL JEM 1011 transmission electron microscope at 80 kV. Images were collected using an AMT digital imaging system with proprietary image capture software (Advanced Microscopy Techniques, Danvers, MA).

5.7 | EV Size and Concentration Measurement

EVs were characterized using tunable resistive pulse sensing (TRPS) qNano instrument (iZON Science, Christchurch, New Zealand), and Nanoparticle tracking Analysis (NTA) through the Nanosight LM10 instrument with 305 mm blue laser (Malvern Panalytical, Malven, UK). Measurements with qNano were done according to manufacturer's protocol using NP300 pore with CPC400 calibration beads. Briefly, upper and lower fluid wells were primed with PBS, and then calibration beads were forced to flow through the nanopore at pressures between 5 and 20 mbar using a variable water-based pressure module. For every experiment, three measurements under three different pressures were taken. The nanopore stretch and the measured voltage at 0 mbar pressure was kept the same between measurements for compatibility. Obtained data analyzed using Control Suite

Software v3.3 from the same manufacturer. For NTA analysis 3 measurement of 30 s were taken from the NanoSight LM10 instrument and exported data was plotted on GraphPad Prism 10. For each experiment, three biological replicates were used per sample.

5.8 | RNA Isolation

RNA was isolated from 37 samples, including 20 EV populations and 17 cell populations from five cell-culture subtrate conditions (0.5 kPa; 2 kPa; 8 kPa; 3D; 2D). Total RNA from cells and cell culture derived EVs was isolated using the miRNeasy mini kit (Qiagen, Hilden, Germany) according to the manufacturers protocol. Ultracentrifuge-purified EVs from cell lines and pelleted cells were lysed with 700 µL of QIAzol Lysis Reagent (Qiagen), followed by chloroform extraction and purification with the miRNeasy kit, with an additional optional DNase treatment (Qiagen). Concentration was assessed by TapeStation (Agilent Technologies, Santa Clara, CA).

5.9 | Library Preparation and RNA Sequencing

Libraries for total RNA-Seq were generated using the Clontech-Takara Smarter Stranded Total RNA-Seq kit v2 (catalog 634413) according to the manufacturer's instructions. Briefly, RNA samples were first converted into cDNA, then adaptors for Illumina sequencing were added through PCR. The PCR products are purified using AMPure Beads (Beckman Coulter, cat# A63881), then ribosomal cDNA was depleted. After depletion, the samples were further amplified using PCR, then purified again using AMPure Beads. Each sample was then qPCR quantified using a KAPA Library Quantification Kit (Roche, cat# 07960140001) and Phix Control Kit V3 (Illumina, cat# FC-110-3001). RNA sequencing was performed with 150 bp paired-end sequencing using an Illumina NextSeq 500 System.

5.10 | RNA-Seq Counts Table Generation

For 3 cell sample conditions (PDAC3 0.5, 2, and 8 kPa), biological replicates were removed due to low RNA quality. Counts tables were generated by processing reads through a pipeline to determine the protein-coding and repeat RNA profile of the samples. Reads were trimmed and quality checked using skewer. Briefly, ends of the reads were trimmed to remove Ns and bases with quality less than 20. After that, the quality scores of the remaining bases were sorted, and the quality at the 20th percentile was computed. If the quality at the 20th percentile was less than 15, the whole read was discarded. In addition, reads shorter than 40 bases after trimming were discarded. If at least 1 of the reads in the pair failed the quality check and had to be discarded, we discarded the mate as well. Quality filtered reads were mapped using STAR aligner (https://github.com/alexdobin/STAR/releases) using human genome (hg38) and assigned to genes (Gencode annotation) and repeat elements (RepeatMasker annotation) using the featureCount function of Subread package with the external Ensembl annotation. Unassigned reads were then remapped to the Repbase consensus sequence. Repeat counts from RepeatMasker annotation and Repbase were added together.

5.11 | Differential Gene Expression Analysis and Gene-Set Enrichment Analysis

For differential gene expression, raw counts data were filtered to keep transcripts with at least 1 raw count observed for at least 1 PDAC sample using DESeq2 (DESeq2 package v1.42.0 in R version 4.3.2) and normalized with DESeq2 default median of ratios followed by Wald tests for differential gene expression on EV subset and the Cell subset separately with the following comparisons 0.5 kPa v 2D; 2 kPa v 2D; 8 kPa v 2D; and 3D v 2D (adjusted p-value cut-off of 0.05). Subsequently, the differential gene expression results (log-fold-change (LFC) values) were analyzed against the Gene Ontology Biological Processes (GOBP) gene set with an enrichment *p*-value cut-off of 0.05 for Gene-set enrichment analysis (GSEA) (R version 4.3.2, script available on githublink)(10.18129/B9.bioc.fgsea). Genes of interest were selected based on the Normalized Enrichment Score (NES) and the leadingEdge analysis.

5.12 | Statistical Analysis

The *p* values were calculated using GraphPad Prism 10 (v10.4.1) student's *t* test, one-way ANOVA. Data are expressed as mean ± S.D or mean ± S.E.M, as appropriate. Statistical analysis was performed in three independent experiments, unless stated otherwise. Log-2 normalization was applied prior to heatmap generation.

Author Contributions

S.I.V., B.A., and R.L.P designed and performed experiments, analyzed the data, and wrote the manuscript. E.T. performed RNA-sequencing. B.A. U.P, J.W., R.L.P., and V.T. generated all computational analysis. S.L.S and D.T.T. supervised the study, contributed to data analysis, and edited the manuscript.

Acknowledgements

We also express our gratitude to all members of the Stott and Ting labs for their thoughtful feedback and assistance with this study. We would also like to thank Mollie Bienstock and Beatriz Marques for their assistance with cell culture. We are grateful to Uyen Ho, Emily Silva, and Danielle Bestoso for administrative support.

Funding

This work was supported by the Warshaw Institute for Pancreatic Cancer Research (R.L.P., S.L.S, S.I.V.), the Burroughs Wellcome Fund (D.T.T.), the NSF PHY-1549535 (D.T.T.), SU2C and Lustgarten Foundation (D.T.T.), ACD-Biotechne (D.T.T). National Cancer Institute under Grant R01-CA226871 and R01CA226871-05S1 (S.L.S); d'Arbeloff MGH Research Scholar Award (S.L.S); American Cancer Society under Grant 132030-RSG-18-108-01-TBG (S.L.S); V Foundation (S.L.S).

Conflicts of Interest

S.L.S serve as a scientific advisory board member for Streck, LLC, unrelated to this work. D.T.T. has received consulting fees from ROME

Therapeutics, Sonata Therapeutics, Leica Biosystems Imaging, PanTher Therapeutics, 65 Therapeutics, and abrdn. D.T.T. is a founder and has equity in ROME Therapeutics, PanTher Therapeutics and TellBio, Inc., which is not related to this work. D.T.T. is on the advisory board with equity for ImproveBio, Inc. and 65 Therapeutics. D.T.T. has received honorariums from Astellas, AstraZeneca, Moderna, and Ikena Oncology that are not related to this work. D.T.T. receives research support from ACD-Biotechne, AVA LifeScience GmbH, Incyte Pharmaceuticals, Sanofi, and Astellas which was not used in this work. D.T.T. and S.L.S's interests were reviewed and are managed by Massachusetts General Hospital and Mass General Brigham in accordance with their conflicts of interest policies. All other authors declare they have no conflicts of interest.

Data Availability Statement

The data that support the findings of this study are available from the corresponding author upon reasonable request.

References

1. R. Liang and G. Song, "Matrix Stiffness-Driven Cancer Progression and the Targeted Therapeutic Strategy," *Mechanobiology in Medicine* 1 (2023): 100013, https://doi.org/10.1016/j.mbm.2023.100013.

2. A. J. Rice, E. Cortes, D. Lachowski, et al., "Matrix Stiffness Induces Epithelial–Mesenchymal Transition and Promotes Chemoresistance in Pancreatic Cancer Cells," *Oncogenesis* 6 (2017): 352, https://doi.org/10.1038/oncsis.2017.54.

3. Y. Shi, L. Cang, X. Zhang, et al., "The Use of Magnetic Resonance Elastography in Differentiating Autoimmune Pancreatitis from Pancreatic Ductal Adenocarcinoma: A Preliminary Study," *European Journal of Radiology* 108 (2018): 13–20, https://doi.org/10.1016/j.ejrad.2018.09.001.

4. Y. Itoh, Y. Takehara, T. Kawase, et al., "Feasibility of Magnetic Resonance Elastography for the Pancreas at 3T," *Journal of Magnetic Resonance Imaging* 43 (2016): 384–390, https://doi.org/10.1002/jmri.24995.

5. M. Ravi, A. Ramesh, and A. Pattabhi, "Contributions of 3D Cell Cultures for Cancer Research," *Journal of Cellular Physiology* 232 (2017): 2679–2697, https://doi.org/10.1002/jcp.25664.

6. A. G. Souza, I. B. B. Silva, E. Campos-Fernandez, et al., "Comparative Assay of 2D and 3D Cell Culture Models: Proliferation, Gene Expression and Anticancer Drug Response," *Current Pharmaceutical Design* 24 (2018): 1689–1694, https://doi.org/10.2174/1381612824666180404152304.

7. S. Breslin and L. Driscoll, "The Relevance of Using 3D Cell Cultures, in Addition to 2D Monolayer Cultures, When Evaluating Breast Cancer Drug Sensitivity and Resistance," *Oncotarget* 7 (2016): 45745.

8. K. Duval, H. Grover, L. H. Han, et al., "Modeling Physiological Events in 2D vs. 3D Cell Culture," *Physiology (Bethesda, Md)* 32 (2017): 266–277.

9. P. A. Kenny, G. Y. Lee, C. A. Myers, et al., "The Morphologies of Breast Cancer Cell Lines in Three-Dimensional Assays Correlate with Their Profiles of Gene Expression," *Molecular Oncology* 1 (2007): 84–96, https://doi.org/10.1016/j.molonc.2007.02.004.

10. Z. N. Abbas, A. Z. Al-Saffar, S. M. Jasim, and G. M. Sulaiman, "Comparative Analysis between 2D and 3D Colorectal Cancer Culture Models for Insights into Cellular Morphological and Transcriptomic Variations," *Scientific Reports* 13 (2023): 18380, https://doi.org/10.1038/s41598-023-45144-w.

11. H. Choi, M. Kim, S. I. Ahn, E.-G. Cho, T. R. Lee, and J. H. Shin, "Regulation of Pigmentation by Substrate Elasticity in Normal human Melanocytes and Melanotic MNT1 human Melanoma Cells," *Experimental Dermatology* 23 (2014): 172–177, https://doi.org/10.1111/exd.12343.

12. A. J. Engler, S. Sen, H. L. Sweeney, and D. E. Discher, "Matrix Elasticity Directs Stem Cell Lineage Specification," *Cell* 126 (2006): 677–689, https://doi.org/10.1016/j.cell.2006.06.044.

13. L. T. Vu, V. Keschrumrus, X. Zhang, et al., "Tissue Elasticity Regulated Tumor Gene Expression: Implication for Diagnostic Biomarkers of Primitive Neuroectodermal Tumor," *PLoS ONE* 10 (2015): 0120336, https://doi.org/10.1371/journal.pone.0120336.

14. M. Reimer, P. Zustiak, S. Sheth, et al., "Intrinsic Response towards Physiologic Stiffness Is Cell-Type Dependent," *Cell Biochemistry and Biophysics* 76 (2018): 197–208, https://doi.org/10.1007/s12013-017-0834-1.

15. F. Pampaloni, E. G. Reynaud, and E. H. K. Stelzer, "The Third Dimension Bridges the Gap between Cell Culture and Live Tissue," *Nature Reviews Molecular Cell Biology* 8 (2007): 839–845, https://doi.org/10.1038/nrm2236.

16. S. Thippabhotla, C. Zhong, and M. He, "3D cell Culture Stimulates the Secretion of in Vivo like Extracellular Vesicles," *Scientific Reports* 9 (2019): 13012, https://doi.org/10.1038/s41598-019-49671-3.

17. B. Wu, D.-A. Liu, L. Guan, et al., "Stiff Matrix Induces Exosome Secretion to Promote Tumour Growth," *Nature Cell Biology* 25 (2023): 415–424, https://doi.org/10.1038/s41556-023-01092-1.

18. A. Sneider, Y. Liu, B. Starich, et al., "Small Extracellular Vesicles Promote Stiffness-mediated Metastasis," *Cancer Research Communications* 4 (2024): 1240–1252, https://doi.org/10.1158/2767-9764.CRC-23-0431.

19. G. Raposo and W. Stoorvogel, "Extracellular Vesicles: Exosomes, Microvesicles, and Friends," *Journal of Cell Biology* 200 (2013): 373–383, https://doi.org/10.1083/jcb.201211138.

20. J. De Toro, L. Herschlik, C. Waldner, and C. Mongini, "Emerging Roles of Exosomes in Normal and Pathological Conditions: New Insights for Diagnosis and Therapeutic Applications," *Frontiers in Immunology* 6 (2015): 203, https://doi.org/10.3389/fimmu.2015.00203.

21. H. Valadi, K. Ekström, A. Bossios, M. Sjöstrand, J. J. Lee, and J. O. Lötvall, "Exosome-mediated Transfer of mRNAs and microRNAs Is a Novel Mechanism of Genetic Exchange between Cells," *Nature Cell Biology* 9 (2007): 654–659, https://doi.org/10.1038/ncb1596.

22. B. Costa-Silva, N. M. Aiello, A. J. Ocean, et al., "Pancreatic Cancer Exosomes Initiate Pre-metastatic Niche Formation in the Liver," *Nature Cell Biology* 17 (2015): 816–826, https://doi.org/10.1038/ncb3169.

23. A. Hoshino, B. Costa-Silva, T.-L. Shen, et al., "Tumour Exosome Integrins Determine Organotropic Metastasis," *Nature* 527 (2015): 329–335, https://doi.org/10.1038/nature15756.

24. V. Luga, L. Zhang, A. M. Viloria-Petit, et al., "Exosomes Mediate Stromal Mobilization of Autocrine Wnt-PCP Signaling in Breast Cancer Cell Migration," *Cell* 151 (2012): 1542–1556, https://doi.org/10.1016/j.cell.2012.11.024.

25. S. A. Melo, H. Sugimoto, J. T. O'Connell, et al., "Cancer Exosomes Perform Cell-Independent microRNA Biogenesis and Promote Tumorigenesis," *Cancer Cell* 26 (2014): 707–721, https://doi.org/10.1016/j.ccell.2014.09.005.

26. H. G. Zhang and W. E. Grizzle, "Exosomes," *The American Journal of Pathology* 184 (2014): 28–41, https://doi.org/10.1016/j.ajpath.2013.09.027.

27. E. Adachi, K. Sakai, T. Nishiuchi, R. Imamura, H. Sato, and K. Matsumoto, "Different Growth and Metastatic Phenotypes Associated with a Cell-Intrinsic Change of Met in Metastatic Melanoma," *Oncotarget* 7 (2016): 70779–70793, https://doi.org/10.18632/oncotarget.12221.

28. Z. Sun, K. Shi, S. Yang, et al., "Effect of Exosomal miRNA on Cancer Biology and Clinical Applications," *Molecular Cancer* 17 (2018): 147, https://doi.org/10.1186/s12943-018-0897-7.

29. Y. Qiu, P. Li, Z. Zhang, and M. Wu, "Insights into Exosomal Non-Coding RNAs Sorting Mechanism and Clinical Application," *Frontiers in Oncology* 11 (2021): 664904, https://doi.org/10.3389/fonc.2021.664904.

30. S. Manier, C.-J. Liu, H. Avet-Loiseau, et al., "Prognostic Role of Circulating Exosomal miRNAs in Multiple Myeloma," *Blood* 129 (2017): 2429–2436, https://doi.org/10.1182/blood-2016-09-742296.

31. J. Skog, T. Würdinger, S. van Rijn, et al., "Glioblastoma Microvesicles Transport RNA and Proteins That Promote Tumour Growth and Provide Diagnostic Biomarkers," *Nature Cell Biology* 10 (2008): 1470–1476, https://doi.org/10.1038/ncb1800.

32. R. L. Porter, S. Sun, M. N. Flores, et al., "Satellite Repeat RNA Expression in Epithelial Ovarian Cancer Associates with a Tumor-immunosuppressive Phenotype," *Journal of Clinical Investigation* 132 (2022): 155931.

33. E. You, P. Danaher, C. Lu, et al., "Disruption of Cellular Plasticity by Repeat RNAs in human Pancreatic Cancer," *Cell* 187 (2024): 7232–7247.e23, https://doi.org/10.1016/j.cell.2024.09.024.

34. S. A. Hinger, D. J. Cha, J. L. Franklin, et al., "Diverse Long RNAs Are Differentially Sorted into Extracellular Vesicles Secreted by Colorectal Cancer Cells," *Cell Reports* 25 (2018): 715–725.e4, https://doi.org/10.1016/j.celrep.2018.09.054.

35. D. T. Ting, D. Lipson, S. Paul, et al., "Aberrant Overexpression of Satellite Repeats in Pancreatic and Other Epithelial Cancers," *Science* 331 (2011): 593–596, https://doi.org/10.1126/science.1200801.

36. K. B. Chiappinelli, P. L. Strissel, A. Desrichard, et al., "Inhibiting DNA Methylation Causes an Interferon Response in Cancer via dsRNA Including Endogenous Retroviruses," *Cell* 162 (2015): 974–986, https://doi.org/10.1016/j.cell.2015.07.011.

37. T. L. Cuellar, A.-M. Herzner, X. Zhang, et al., "---Silencing of Retrotransposons by SETDB1 Inhibits the Interferon Response in Acute Myeloid Leukemia--," *Journal of Cell Biology* 216 (2017): 3535–3549, https://doi.org/10.1083/jcb.201612160.

38. D. Roulois, H. Loo Yau, R. Singhania, et al., "DNA-Demethylating Agents Target Colorectal Cancer Cells by Inducing Viral Mimicry by Endogenous Transcripts," *Cell* 162 (2015): 961–973, https://doi.org/10.1016/j.cell.2015.07.056.

39. M. L. Stone, K. B. Chiappinelli, H. Li, et al., "Epigenetic Therapy Activates Type I Interferon Signaling in Murine Ovarian Cancer to Reduce Immunosuppression and Tumor Burden," *Proceedings of the National Academy of Sciences* 114 (2017): E10981–E10990, https://doi.org/10.1073/pnas.1712514114.

40. A. Tanne, L. R. Muniz, A. Puzio-Kuter, et al., "Distinguishing the Immunostimulatory Properties of Noncoding RNAs Expressed in Cancer Cells," *Proceedings of the National Academy of Sciences* 112 (2015): 15154–15159, https://doi.org/10.1073/pnas.1517584112.

41. S. Patwardhan, P. Mahadik, O. Shetty, and S. Sen, "ECM Stiffness-Tuned Exosomes Drive Breast Cancer Motility through Thrombospondin-1," *Biomaterials* 279 (2021): 121185, https://doi.org/10.1016/j.biomaterials.2021.121185.

42. K. Parihar, J. Nukpezah, D. V. Iwamoto, P. A. Janmey, and R. Radhakrishnan, "Data Driven and Biophysical Insights Into the Regulation of Trafficking Vesicles By Extracellular Matrix Stiffness," *Iscience* 25 (2022): 104721.

43. L. Indolfi, M. Ligorio, D. T. Ting, et al., "A Tunable Delivery Platform to Provide Local Chemotherapy for Pancreatic Ductal Adenocarcinoma," *Biomaterials* 93 (2016): 71–82, https://doi.org/10.1016/j.biomaterials.2016.03.044.

44. M. Ligorio, S. Sil, J. Malagon-Lopez, et al., "Stromal Microenvironment Shapes the Intratumoral Architecture of Pancreatic Cancer," *Cell* 178 (2019): 160–175.e27, https://doi.org/10.1016/j.cell.2019.05.012.

45. J. A. Welsh, D. C. I. Goberdhan, L. O'Driscoll, et al., "Minimal Information for Studies of Extracellular Vesicles (MISEV2023): from Basic to Advanced Approaches," *Journal of Extracellular Vesicles* 13 (2024): 12404, https://doi.org/10.1002/jev2.12404.

46. A. Solovyov, N. Vabret, K. S. Arora, et al., "Global Cancer Transcriptome Quantifies Repeat Element Polarization between Immunotherapy Responsive and T Cell Suppressive Classes," *Cell Reports* 23 (2018): 512–521, https://doi.org/10.1016/j.celrep.2018.03.042.

47. E. Reátegui, K. E. van der Vos, C. P. Lai, et al., "Engineered Nanointerfaces for Microfluidic Isolation and Molecular Profiling of Tumor-specific Extracellular Vesicles," *Nature Communications* 9 (2018): 175, https://doi.org/10.1038/s41467-017-02261-1.

48. B. Emon, J. Bauer, Y. Jain, B. Jung, and T. Saif, "Biophysics of Tumor Microenvironment and Cancer Metastasis-a Mini Review," *Computational and Structural Biotechnology Journal* 16 (2018): 279–287.

49. C. Chiasson-MacKenzie, Z. S. Morris, Q. Baca, et al., "NF2/Merlin Mediates Contact-dependent Inhibition of EGFR Mobility and Internalization via Cortical Actomyosin," *Journal of Cell Biology* 211 (2015): 391–405, https://doi.org/10.1083/jcb.201503081.

50. S. Acevedo-Acevedo and W. C. Crone, "Substrate Stiffness Effect and Chromosome Missegregation in hIPS Cells," *Journal of Negative Results in BioMedicine* 14 (2015): 22, https://doi.org/10.1186/s12952-015-0042-8.

51. P. M. Gilbert, K. L. Havenstrite, K. E. G. Magnusson, et al., "Substrate Elasticity Regulates Skeletal Muscle Stem Cell Self-Renewal in Culture," *Science* 329 (2010): 1078–1081, https://doi.org/10.1126/science.1191035.

52. G. Skogberg, J. Gudmundsdottir, S. van der Post, et al., "Characterization of human Thymic Exosomes," *PLoS ONE* 8 (2013): 67554, https://doi.org/10.1371/journal.pone.0067554.

53. L. Geis-Asteggiante, A. T. Belew, V. K. Clements, et al., "Differential Content of Proteins, mRNAs, and miRNAs Suggests That MDSC and Their Exosomes May Mediate Distinct Immune Suppressive Functions," *Journal of Proteome Research* 17 (2018): 486–498, https://doi.org/10.1021/acs.jproteome.7b00646.

54. C. Villarroya-Beltri, C. Gutiérrez-Vázquez, F. Sánchez-Cabo, et al., "Sumoylated hnRNPA2B1 Controls the Sorting of miRNAs into Exosomes through Binding to Specific Motifs," *Nature Communications* 4 (2013): 2980, https://doi.org/10.1038/ncomms3980.

55. C. Villarroya-Beltri, F. Baixauli, C. Gutierrez-Vazquez, F. Sanchez-Madrid, and M. Mittelbrunn, "Sorting It out: Regulation of Exosome Loading," *Seminars in Cancer Biology* 28 (2014): 3–13, https://doi.org/10.1016/j.semcancer.2014.04.009.

56. D. Perez-Hernandez, C. Gutiérrez-Vázquez, I. Jorge, et al., "The Intracellular Interactome of Tetraspanin-Enriched Microdomains Reveals Their Function as Sorting Machineries Toward Exosomes," *Journal of Biological Chemistry* 288 (2013): 11649–11661, https://doi.org/10.1074/jbc.M112.445304.

57. J. Perez-Boza, M. Lion, and I. Struman, "Exploring the RNA Landscape of Endothelial Exosomes," *RNA* 24 (2018): 423–435.

58. R. Zhou, K. K. Chen, J. Zhang, et al., "The Decade of Exosomal Long RNA Species: an Emerging Cancer Antagonist," *Molecular Cancer* 17 (2018): 75, https://doi.org/10.1186/s12943-018-0823-z.

59. T. Kishikawa, M. Otsuka, T. Yoshikawa, et al., "Quantitation of Circulating Satellite RNAs in Pancreatic Cancer Patients," *JCI Insight* 1 (2016): 86646, https://doi.org/10.1172/jci.insight.86646.

60. S. W. Criscione, Y. Zhang, W. Thompson, J. M. Sedivy, and N. Neretti, "Transcriptional Landscape of Repetitive Elements in Normal and Cancer human Cells," *BMC Genomics [Electronic Resource]* 15 (2014): 583, https://doi.org/10.1186/1471-2164-15-583.

61. X. D. Ho, H. G. Nguyen, L. H. Trinh, et al., "Analysis of the Expression of Repetitive DNA Elements in Osteosarcoma," *Frontiers in Genetics* 8 (2017): 193, https://doi.org/10.3389/fgene.2017.00193.

62. M. De Cecco, T. Ito, A. P. Petrashen, et al., "L1 Drives IFN in Senescent Cells and Promotes Age-associated Inflammation," *Nature* 566 (2019): 73–78, https://doi.org/10.1038/s41586-018-0784-9.

63. S. Rocha, J. Carvalho, P. Oliveira, et al., "3D Cellular Architecture Affects MicroRNA and Protein Cargo of Extracellular Vesicles," *Advanced Science* 6 (2019): 1800948, https://doi.org/10.1002/advs.201800948.

64. A. Villasante, A. Marturano-Kruik, S. R. Ambati, et al., "Recapitulating the Size and Cargo of Tumor Exosomes in a Tissue-Engineered Model," *Theranostics* 6 (2016): 1119–1130, https://doi.org/10.7150/thno.13944.

65. S. Guo, L. Debbi, B. Zohar, et al., "Stimulating Extracellular Vesicles Production from Engineered Tissues by Mechanical Forces," *Nano Letters* 21 (2021): 2497–2504, https://doi.org/10.1021/acs.nanolett.0c04834.

66. C. Almeria, R. Weiss, M. Keck, V. Weber, C. Kasper, and D. Egger, "Dynamic Cultivation of human Mesenchymal Stem/Stromal Cells for the Production of Extracellular Vesicles in a 3D Bioreactor System," *Biotechnology Letters* 46 (2024): 279–293, https://doi.org/10.1007/s10529-024-03465-4.

67. S. M. Kronstadt, D. B. Patel, L. J. Born, et al., "Mesenchymal Stem Cell Culture within Perfusion Bioreactors Incorporating 3D-Printed Scaffolds Enables Improved Extracellular Vesicle Yield with Preserved Bioactivity," *Advanced Healthcare Materials* 12 (2023): 2300584, https://doi.org/10.1002/adhm.202300584.

68. H. Jing, W. Cheng, Z.-Y. Li, et al., "Early Evaluation of Relative Changes in Tumor Stiffness by Shear Wave Elastography Predicts the Response to Neoadjuvant Chemotherapy in Patients with Breast Cancer," *Journal of Ultrasound in Medicine* 35 (2016): 1619–1627, https://doi.org/10.7863/ultra.15.08052.

69. J. P. Miller, B. H. Borde, F. Bordeleau, et al., "Clinical Doses of Radiation Reduce Collagen Matrix Stiffness," *APL Bioengineering* 2 (2018): 031901, https://doi.org/10.1063/1.5018327.

Supporting Information

Additional supporting information can be found online in the Supporting Information section.

Supporting File 1: smll72185-sup-0001-SuppMat.docx.

Supporting File 2: smll72185-sup-0002-FigureS1.docx.